

## NEUTRON DIFFRACTION FROM CLAY-WATER SYSTEMS

D. J. CEBULA, R. K. THOMAS

Physical Chemistry Laboratory, South Parks Rd., Oxford OX1 3QZ

S. MIDDLETON, R. H. OTTEWILL

School of Chemistry, Bristol University, Cantock's Close, Bristol BS8 1TS

AND

J. W. WHITE

Institut Laue-Langevin, BP 156, Centre de Tri, Grenoble 38042 Cedex, France

(Received 9 March 1978)

**Abstract**—The use of neutron diffraction to determine some of the structural properties of montmorillonite–water systems at low water concentrations is described. The samples were prepared by compression or suction to give clay samples with between one and three molecular layers of water between the plates.

About 10% of the platelets in the clay are randomly oriented. The remainder are partially oriented in the plane of the sample, with an angular spread of 40° about the mean orientation. It is suggested that these oriented domains are formed from the larger platelets present in the system. The Bragg diffraction pattern is better explained by a disordered lattice model rather than by a mixture model with small particles having a well-defined lattice spacing. We have fitted both the intensities of (00) reflections and the shape of the (001) reflection quantitatively to a model which allows for a Gaussian spread of platelet spacing about a mean value. The half width of the spread is about 10% of the lattice spacing.

No significant structural differences are found between Li, Na, K, and Cs montmorillonites. The method of preparation has no effect on the structural properties of the large platelet particles but does affect the randomly oriented fraction. The lattice spacing of the latter appears to be better defined for samples prepared by compression.

Experiments on the variation of lattice spacing with humidity indicate that the structural model we have used is adequate except at humidities where the system is changing over from one to two, or two to three water layers.

**Key Words**—Humidity, Montmorillonite, Neutron, Quasielastic.

### INTRODUCTION

This paper describes neutron diffraction experiments to determine some of the structural properties of compacted clay–water samples. The work is part of a study of the dynamical properties of water in clays using neutron quasielastic scattering, the structural information being essential for a quantitative analysis of the quasielastic scattering experiments. The results on the dynamical properties of water in clays will be described in another paper.

The properties of clay–water systems have been extensively reviewed, for example, by Graham (1964), Anderson (1966), and van Olphen (1977). A schematic diagram of the generally accepted features of the system is given in Figure 1 and should be compared with the electron micrographs of a dry sample and of platelets in the sol in Figure 2. Parameters which might be considered to characterize the system are the frequencies of occurrence of different types of fault in the structure and some quantitative measure of the stacking. Many of the faults result from the spread in the diameters of the clay platelets from which the sample is prepared (Figure 2). Such faults may be classified as (A) voids, (B) edge to face stacking, (C) regions of gross folding, (D) ordered domains, and (E) regions of disordered stacking, the labels being marked on the appropriate regions of Figure 1. Another parameter which

is important for the interpretation of our experiments on the dynamics of water molecules is the spread in orientation of the platelets.

The crystalline structure of a montmorillonite platelet, shown in the inset of Figure 1, has been determined by X-ray powder diffraction (Brown, 1961). X-ray studies have given the atomic positions in the clay unit cell, the position of exchangeable cations in both the clay structure and the interlamellar regions, but little information on the position of the protons in the system. This is because the scattering from hydrogen atoms is inherently weak and because these atoms are known to be moving rapidly. The dynamical properties of protons in several clay–water systems have been studied by nuclear magnetic resonance (Hougardy et al., 1976) and will be discussed further in our paper on neutron quasielastic scattering.

Much less work has been done using diffraction techniques to study the overall structure of two dimensional platelets packed in three dimensions. Models based on the effect of the small size of ordered domains (D) and platelet bending (C) have been used to explain some of the features of X-ray patterns (Güven, 1975; Williams and Garey, 1974). Random irregularities in the spacing of the platelets (E) have a strong effect on the diffraction pattern and also have been used to interpret X-ray data (Kodama et al., 1971). In a recent X-ray study of

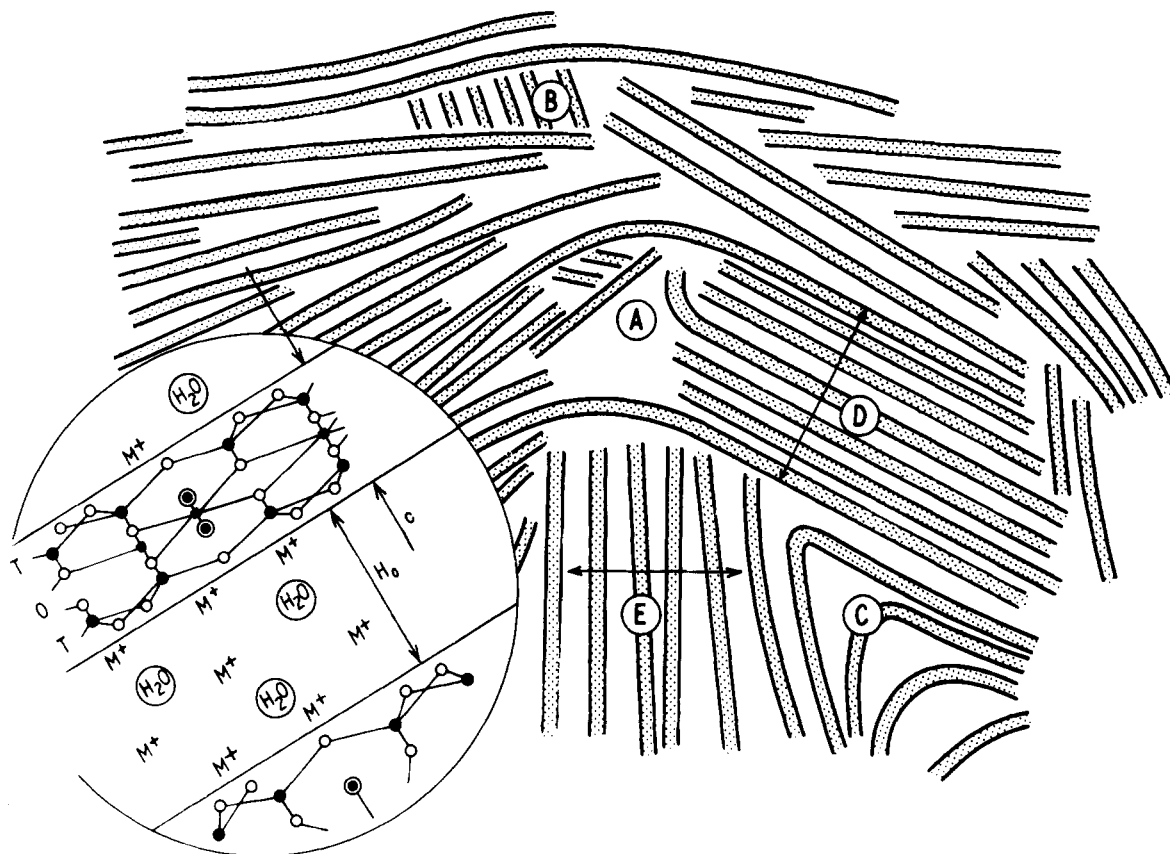


Fig. 1. Schematic structure of a clay-water system showing the bulk arrangements of clay platelets (shaded) and the structural defects A, B, C, D, E referred to in the text. The inset shows the crystalline structure of montmorillonite ○ = O; ● = Si; ■ = Al(Mg, Fe, etc.); ⊙ = OH; M<sup>+</sup> = Li<sup>+</sup>, Na<sup>+</sup>, K<sup>+</sup>, Cs<sup>+</sup>; T, tetrahedral coordination; O, octahedral coordination; H<sub>0</sub> = water space (Å); c = clay platelet thickness, 9.6 Å.

phyllosilicates Plançon and Tchoubar (1977) have calculated the effect of defects similar to these on (hk0) reflections. Taylor and Norrish (1966) and Tchalenko et al. (1971) have examined the spread of platelet orientations by X-ray powder diffraction but the difficulty in determining this spread is in correcting for the absorption of the X-rays which can be overcome only by using very small samples and X-rays of different wavelengths.

Void formation (A in Figure 1) in dry clays has been studied by sorption of gases into both pore and interlamellar regions (Aylemore, 1977; Diamond, 1971). Norrish (1954) has suggested that edge to edge interactions contribute significantly to the properties and structure of montmorillonite-water systems in the gel state, and Rowell (1965) has related edge to face structures to void formation in samples that have suffered some lattice collapse. Fink (1977) has proposed methods to reduce the likelihood of edge to face structures in gels.

Neutron scattering may be used to study both the structure of a system (by neutron diffraction or small

angle scattering) and its dynamical properties (neutron quasielastic and inelastic scattering) (Willis, 1972). In comparison with X-ray diffraction, neutron diffraction has several advantages for the study of heterogeneous systems such as the clays. First, attenuation of a neutron beam in a sample is much less than for X-rays. The 'absorption' length for neutrons passing through a clay containing two molecular layers of water between platelets is approximately 30 mm but for X-rays is only about 0.1 mm. This means that, for practical examples of oriented clays, neutrons will be scattered equally from internal and external parts of the sample. Large samples are used for structural determinations to produce scattering of adequate intensity so that external surface effects become negligible. Because small samples must be used for X-ray experiments, X-ray powder diffraction patterns may be dominated by structural properties which are not at all representative of the bulk material. It is known, for example, that clay samples prepared by shearing show preferential orientation of the platelets (Mitchell, 1953), presumably at the surface of the sample. The ratio of the external surface to the

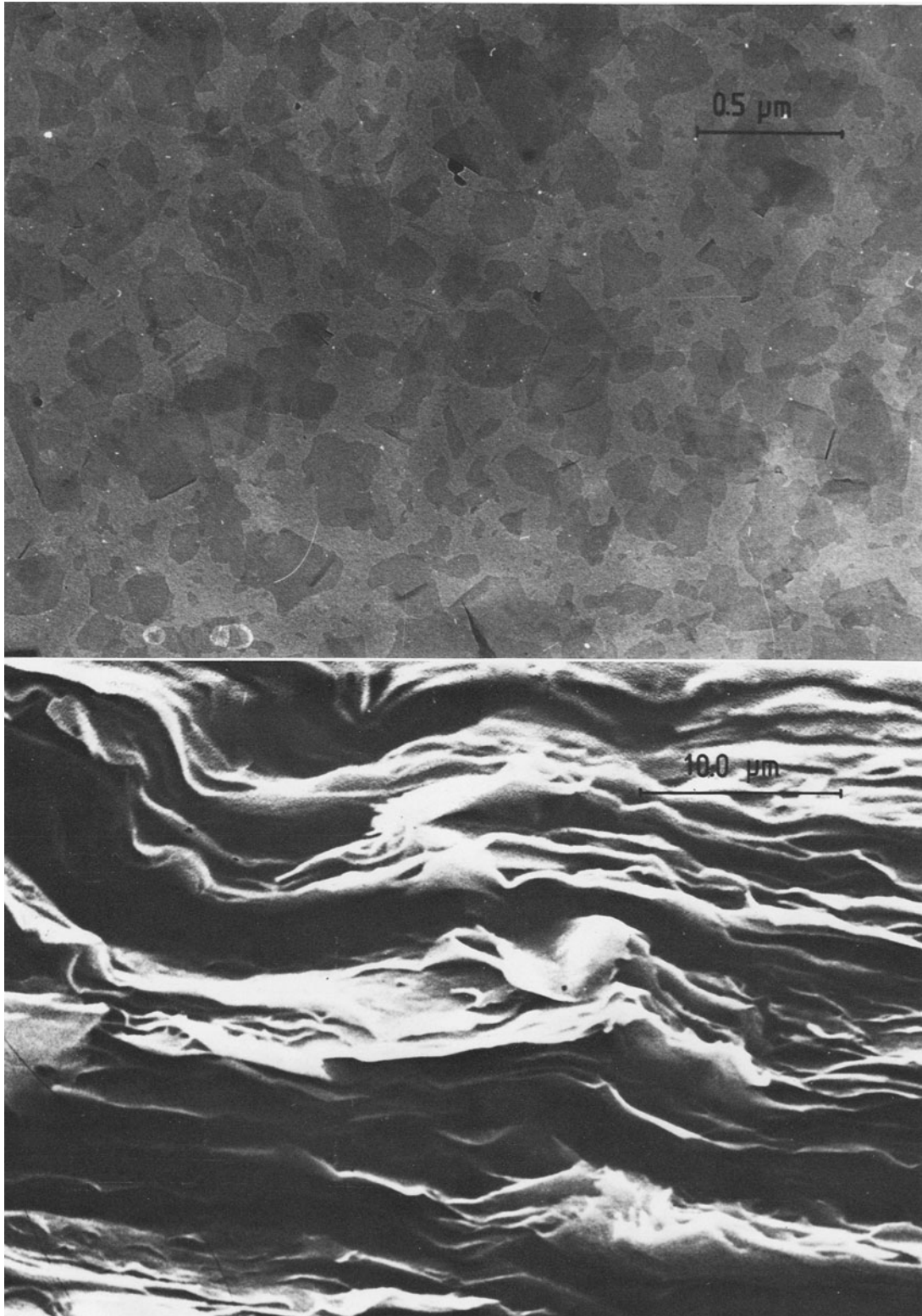


Fig. 2. Electron micrographs of lithium montmorillonite in water. The first picture is taken from a sol of very dilute clay concentration (0.01%). Here the magnification is such as to be able to observe directly the larger single platelets. Note the wide range of diameters of the plates and their jagged appearance. This photograph was taken in transmission mode. The second picture is taken in scanning mode. It shows a photograph of a fractured dried out clay sample. The general structure of faults can clearly be seen.



Table 1. Neutron and X-ray scattering data.

Element	Neutrons <sup>1</sup>		X-Rays <sup>2</sup>
	$b \cdot 10^{12}$ cm	$\sigma \cdot 10^{24}$ cm <sup>2</sup>	$f_x \cdot 10^{12}$ cm
H	-0.374	81.5	0.28
D	0.667	7.6	0.28
O	0.58	4.24	2.25
Al	0.35	1.5	3.65
Si	0.42	2.2	3.95

<sup>1</sup>  $b$  = coherent scattering length for neutrons;  $\sigma$  = total cross section.

<sup>2</sup> Form factor  $f_x$  is for X-rays at  $\sin \theta = 0$ .

mass should be kept as small as possible by increasing the size of the sample. X-ray powder diffraction can be done from large samples but absorption leads to large attenuation effects which are difficult to correct especially when measuring the spread in platelet-orientation. The second property of neutrons is that they are scattered relatively strongly by light atoms (see Table 1). Hydrogen and deuterium scatter with different phases and amplitudes and further structural information can be obtained therefore by using isotopic substitution or H-D scattering contrast as controllable variables. Finally, it is relatively easy to obtain neutrons of longer wavelengths ( $0.5 < \lambda$  (Å)  $< 30.0$ ) suitable for small angle scattering experiments (Jacrot, 1976). These may be used to study the long repeat spacings found in clay-water systems and are of particular value for following the swelling of clays to the gel and sol states. Preliminary results of neutron small angle scattering from clay-water sols are described by Cebula et al. (1978).

No neutron diffraction experiments on aqueous dispersion of clays in water have been published. Adams et al. (1976) have done neutron diffraction from kaolinites intercalated with organic compounds and have successfully determined positions of hydrogen atoms in these systems.

## EXPERIMENTAL METHODS

### Preparation of samples

The raw clay material used was bentonite from Clay Spur, Wyoming (A.P.I. No. 26). Standard techniques described elsewhere by Callaghan and Ottewill (1974) were used to remove residual organic compounds and traces of undesirable heavy metal cations. Experiments were done using Li, Na, K, and Cs as homionic forms of montmorillonite.

Two methods were used to prepare the compacted samples. In the first method, a specialized apparatus was used to compress clay dispersions at constant pressure so that the clay platelets were aligned against a millipore filter (Barclay and Ottewill, 1970). In this method a number of compression-decompression cycles could be carried out in order to improve the regularity of the arrangement of the platelets. The milli-

pore filter also provided a robust support for the sample and thus facilitated its removal from the apparatus. In the second method, water was sucked out of the sol through a filter, approximately as described by Shaw (1972). Both methods give samples with a spacing of about 20 Å (2.0 g H<sub>2</sub>O/g clay). Finally, the samples were dried down to a water content of less than 0.3 g H<sub>2</sub>O/g clay, corresponding to approximately three molecular layers of water between the platelets. The number of cations also present between the layers is determined by the cation exchange capacity.

The sizes of sample varied from 1 to 3 cm in diameter and were chosen to contain sufficient clay to transmit about 95% of the incident neutron beam. At this transmission secondary scattering events are negligible and so no complicated corrections for this are necessary. Typical samples were 0.5–1.0 mm thick, with water layer thicknesses ( $H_0$  in Figure 1) of up to 10 Å; this value can be compared with 9.6 Å for the thickness of the single montmorillonite platelet (C in Figure 1).

### Sample environment

The adsorption isotherms for water vapor into the montmorillonite used in this work have not been measured. For comparison with the diffraction results it is assumed that they are similar to those on other montmorillonites (Mooney et al., 1952; Keren and Shainberg, 1975). The water content of the sample can be fixed therefore by choice of the appropriate relative humidity and temperature. To control the temperature and relative humidity of the sample during experiments a special aluminum chamber was made. Thin aluminum is transparent to neutrons, so windows were machined in the walls of the chamber allowing passage of incident and scattered neutrons to and from the sample. The chamber was airtight except for a gas inlet and outlet through which was circulated air at a known relative humidity produced by bubbling the air through a suitable saturated salt solution with a small diaphragm pump. Salt solutions and their relative humidities have been tabulated by O'Brien (1948). The temperature of both the sample chamber and salt solution was controlled by constant temperature jackets. Samples were considered to have reached equilibrium when no further change in their diffraction pattern could be detected. Changing the number of water layers in a sample took about 6 hr.

### Neutron diffractometers

Three neutron diffractometers were used:

- (1) Guide tube, 7H2R at A.E.R.E. Harwell (Haywood and Worcester, 1973).  
Incident wavelength,  $\lambda = 4.73$  Å.
- (2) D16 at Institut Laue-Langevin (I.L.L.), Grenoble (Institut Laue-Langevin, 1977).  
Incident wavelength,  $\lambda = 4.63$  Å.

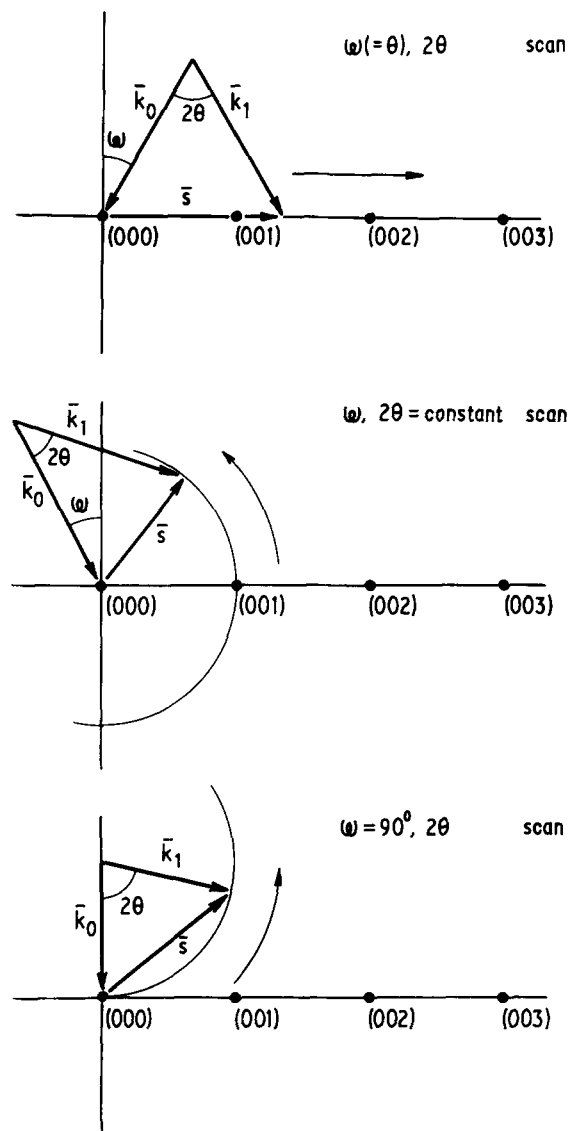


Fig. 3. Loci of scans through reciprocal space. The lattice is shown as a series of dots and the direction of the scans is indicated.  $k_0$ ,  $k_1$  are the wave vectors of the incident and scattered neutrons.  $s = k_1 - k_0$ .

These are single crystal type diffractometers with a detector which can be scanned in a plane, moving through an angle of  $2\theta$  with respect to the incident beam. The sample can be rotated about the same axis as the detector. The angular resolution of each machine can be varied by the use of slits before and after the sample.

- (3) D11, I.L.L. Grenoble (Schmatz et al., 1974).  
Incident wavelength,  $4.0 < \lambda < 16 \text{ \AA}$ .

This instrument has a two-dimensional multidetector ( $64 \times 64 \text{ cm}^2$ ) with its center on the line of the incident beam. Small angle scattering close to the transmitted unscattered beam as well as Bragg spots or Debye-Scherrer rings can be measured in two dimensions in

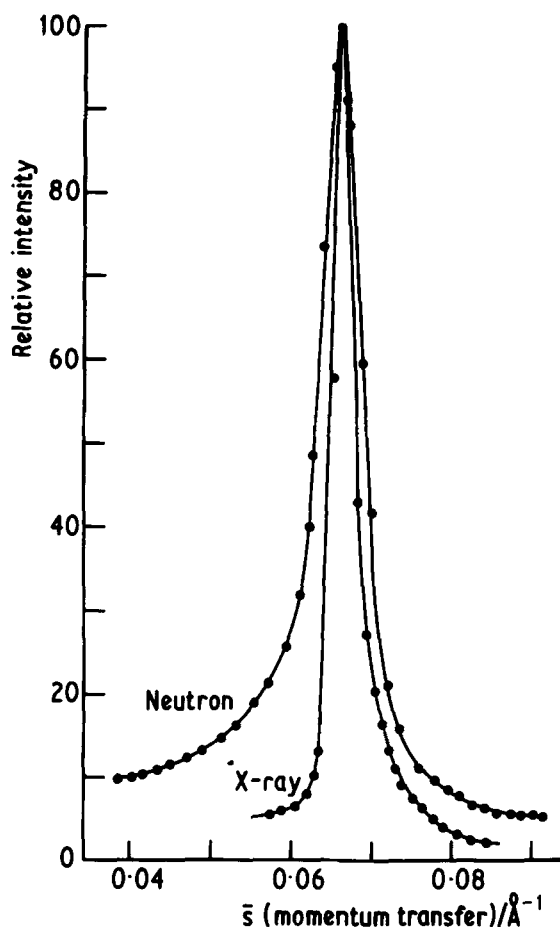


Fig. 4. Comparison of (001) reflections from a lithium-montmorillonite sample obtained by neutron and X-ray diffraction. The plots have been transformed to  $s$  because the wavelength for the two experiments was different. (RH = 76%,  $d = 15.1 \text{ \AA}$ )

a single exposure. This is similar to a normal Debye-Scherrer X-ray camera but with the sensitive area close to the primary beam.

## RESULTS

Three types of diffraction experiment were done and are treated separately below. The loci of these scans through the reciprocal lattice are summarized in Figure 3.

### Normal crystal diffraction: $\omega$ , $2\theta$ scan

Starting with the plane of the sample in line with both the beam and the detector, the sample orientation was changed by  $\omega(= \theta)$  and the scattering angle between beam and detector by  $2\theta$ . This experiment gives a conventional diffraction pattern of the (001) reflections. Though the range of  $2\theta$  used would include five orders, usually only the (001) reflection was observed and that was always very broad compared with the resolution of the machine. At higher angles there was just a high, flat background. X-ray patterns obtained for identical

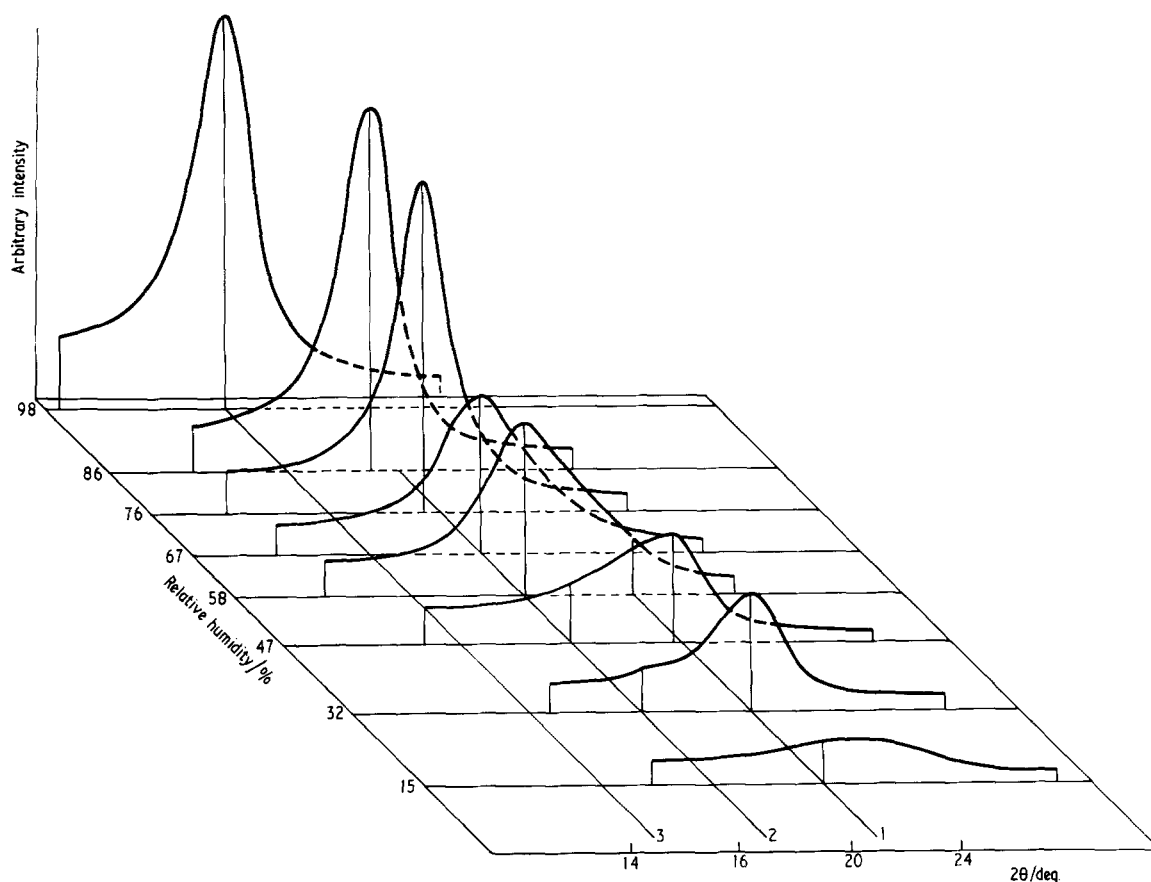


Fig. 5. Diagram showing (001) reflections in the neutron diffraction pattern at various relative humidities from a compacted lithium-montmorillonite-water sample. Background scattering from the sample humidification chamber has been subtracted.

samples usually gave up to four orders of reflections with much narrower peaks. The different appearances of the first reflection (001) in neutron and X-ray patterns from the same sample are shown in Figure 4. The X-ray pattern is characteristic of a well-ordered structure while the neutron pattern is characteristic of a highly disordered structure (see discussion below). This supports the suggestion made in the introduction that an advantage of neutron scattering is that it observes the average, less well ordered structure, of the whole sample, while X-ray diffraction is from better ordered parts of the clay close to the surface of the sample.

Neutron diffraction patterns of this type were recorded at several relative humidities and a set of results for the lithium-montmorillonite-water system is shown in Figure 5.

The patterns shown here are from samples prepared by compression using two decompression-compression cycles. No difference for this type of pattern was seen between compression samples and samples prepared by suction. Likewise no difference was seen between the patterns from Li, Na, K, or Cs samples other than the expected changes in the basal spacing associated

with each ion. As the relative humidity increases there is a stepwise increase in the thickness of the water layer from one to two to three molecular layers. Because the neutron reflections are very broad they overlap, but the best quantitative explanation of the overall peak shape at any given humidity is that it is composed of one or more peaks arising from diffraction from domains having spacings corresponding to one, two, or three layers of water. This is shown by the asymmetry of the composite peak at relative humidities of 47% and 58% (Figure 5). They both appear to be made up of at least two diffraction lines. Another feature that can be seen in Figure 5 is the decrease of intensity of the peak with relative humidity. This is caused by the change in the structure factor of the reflection as a function of water content. The background also decreases with relative humidity because it arises largely from incoherent scattering by the protons in the system. In similar experiments on samples having  $D_2O$  instead of  $H_2O$  in the water layers no incoherent scattering was recorded but also no reflections were seen at all. This is because, unlike an  $H_2O$  layer, the scattering length density of a  $D_2O$  layer is positive and comparable with that of a clay

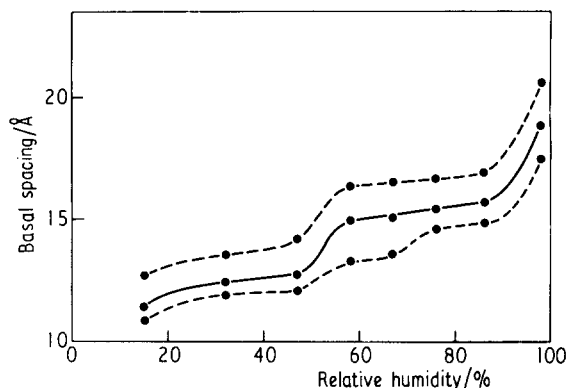


Fig. 6. Plot of basal spacing (peak position represented by —) and skewness of reflections from Figure 5. Here the skewness (----) is taken as the half width of the peak at half height above the background. Note the reversal in skewness as the relative humidity changes from 47% to 58%. At 47% the bulk of the peak is on the low  $2\theta$  side indicating the presence of  $d$  spacings larger than the mean. At 58% the larger basal spacing has become the mean and the asymmetry on the high  $2\theta$  side shows the existence of basal spacings smaller than the mean.

platelet. The contrast of the clay in  $H_2O$  is therefore much greater than in  $D_2O$ . This reduction in contrast accounts for the very small structure factors for both  $D_2O$  samples and samples containing very little  $H_2O$ .

Figure 6 shows the variation of the basal spacing and full width at half maximum of the (001) reflection with relative humidity. The information for this figure is calculated from the reflections shown in Figure 5. Figure 6 shows that, at least on the plateaus of the step line curves, the number of water layers between platelets is well defined. This is deduced from the relatively narrow and symmetrical shape of the diffraction peaks at these humidities. In the region of changeover from one to two molecular layers of water between plates (relative humidities of 47% to 58%) more than one diffraction maximum must be present to account for the width and shape of the observed lines.

#### Rocking curves: $\omega$ , $2\theta = \text{constant scan}$

The detector was set at the angle,  $2\theta$ , corresponding to the 001 reflection and the sample rotated through an angle  $\omega$  with respect to the incident beam. This rocking curve experiment in principle measures directly the spread in the orientations of regions in the sample where platelets are stacked together. When the orientation of the sample is such that the plane of the sample is parallel to the incident beam ( $\omega = 0$ ) or to the detected beam ( $\omega = 2\theta$ ), the intensity of the detected beam is strongly reduced because, in these positions, the path length of the beam through the sample is very long. From the thickness and the transmission coefficient of the sample, measured as described in the Appendix, Part 1, an attenuation factor can be calculated for all  $\omega$  and  $2\theta$  except very close to  $\omega = 0$  and  $\omega = 2\theta$ .

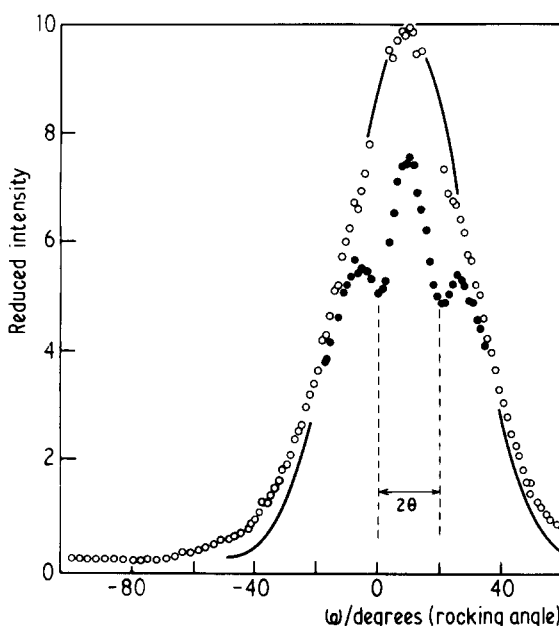


Fig. 7. Rocking curves for lithium montmorillonite (RH = 32%,  $d = c + H_0 = 12.1 \text{ \AA}$ ).  $\bullet$  = observed data,  $\circ$  = data corrected for attenuation. — = Gaussian + flat background.

Details of the calculation are given in the Appendix, Part 2.

A typical measured rocking curve is shown in Figure 7 with the corresponding curve after the attenuation corrections have been applied. The small incoherent scattering background has been subtracted. The full width of the peak at half its maximum above the flat wings is a convenient measure of the mean mosaic spread in the sample. This has the same value of about  $40^\circ$  for both compression and suction samples. It is also independent of exchanged cation. The spread has approximately the shape of a Gaussian superimposed on a flat 'background.' The significance of the 'background' is described below in connection with the relative 'powder' and 'crystal' contents of the sample.

#### Powder diffraction: $\omega = 90^\circ$ , $2\theta$ scan in two dimensions

The third type of experiment was done on the neutron small angle camera, D11. Both sample and multidetector are perpendicular to the incoming beam, thus giving a diffraction pattern in transmission. An isometric picture of the counts recorded in each counter of the two-dimensional detector bank is shown in Figure 8(a). A complete Debye-Scherrer ring is observed showing that at least some of the clay platelet stacks are randomly oriented. Since the sample is perpendicular to the beam this reflection corresponds to parts of the rocking curve (Figure 7) at  $\omega = \pm 90^\circ$  which are flat and not very intense. We attribute the appearance of a complete Debye-Scherrer ring to powderlike elements in

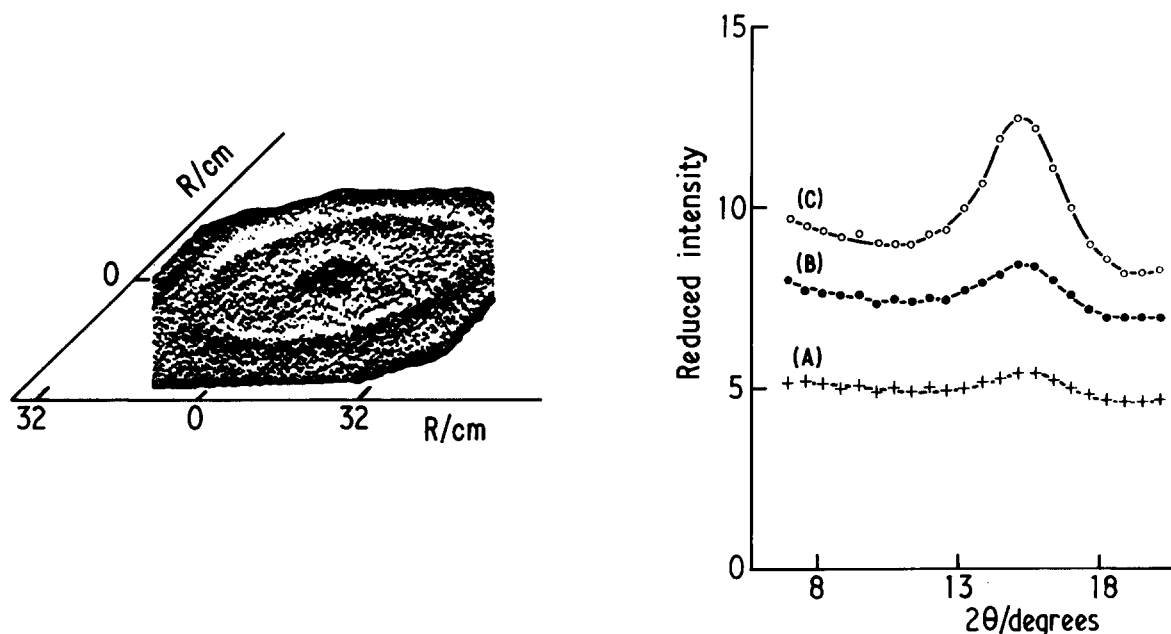


Fig. 8. Transmission diffraction pattern (a) obtained from a lithium-montmorillonite on the camera D11. The central square is the shadow cast by the incident beam stop protecting the counter. The Debye-Scherrer ring is seen clearly. After suitable correction of the 2-D pattern, radial integration gives curves of the type shown in (b). Lithium montmorillonite (RH = 76%,  $d = 15.1 \text{ \AA}$ ).  $\circ$  = twice compressed sample,  $\bullet$  = once compressed,  $+$  = suction sample.

the structure. The widths of these diffraction rings are comparable with the machine resolution.

In this experiment, unlike the others, samples prepared by the two different methods gave different results. In Figure 8(b) are shown intensities integrated around the Debye-Scherrer ring at various radii away from the unscattered beam. The scale is converted from radius to angle of scatter,  $2\theta$ . The samples used were lithium-montmorillonite respectively sucked (A), once compressed (B), and twice compressed (C). The more intense peak observed for the twice compressed sample shows that the degree of ordered conformation within the randomly oriented fraction of the clay is increased by compression.

#### DISCUSSION

The appearance of a Bragg diffraction pattern indicates that there is some degree of order within stacks of clay platelets in the clay-water samples. In every case there is a strong, though broad, (001) reflection but no higher orders can be distinguished. The width of a diffraction line is usually taken to be inversely proportional to the crystallite size, being given by the Scherrer formula (Guinier, 1963). Applying this to the observed width of the (001) reflection shows that the average stack contains about seven platelets.

This small crystallite model is not a good description of the system. First, considering the large diameter of the platelets, the calculated thickness of composite platelet stacks is so small that a large number of dis-

ordered regions would have to be present in between domains to accommodate all the platelets. For example, in addition to small pockets of high order such as (D) in Figure 1, there has to be interleaving of the platelets in regions such as (A) and (B) in Figure 1 which are better regarded as amorphous. Second, the shape of the 001 reflection is markedly asymmetric and this cannot be explained in terms of particle size effects.

The faults listed earlier in the paper lead to irregularities in the positions of clay platelets on the lattice. If, for example, the clay platelets are not all equally spaced the condition for Bragg diffraction is less well defined and the pattern will be of generally poorer quality. It is also likely that no two platelets will be perfectly parallel over all their area, leading to wedgelike channels, again giving rise to poorer definition of lines in the diffraction pattern. A more convenient description of the lattice is in terms of a distribution of basal spacings about a mean value.

A reasonable model of the clay is that of platelets stacked irregularly along the axis of a one-dimensional lattice, a platelet lying at a distance  $d(1 \pm f(\delta))$  from the previous one where  $f(\delta)$  is much smaller than unity. The chance of  $f(\delta)$  having a particular value is given by a suitable distribution function. The simplest such function which accounts for the observations is a Gaussian which can be characterized by a single parameter,  $\delta$ , related to the halfwidth (see Appendix, Part 3). A Gaussian distribution has the advantage that it is easily incorporated into an analytical expression for the dif-



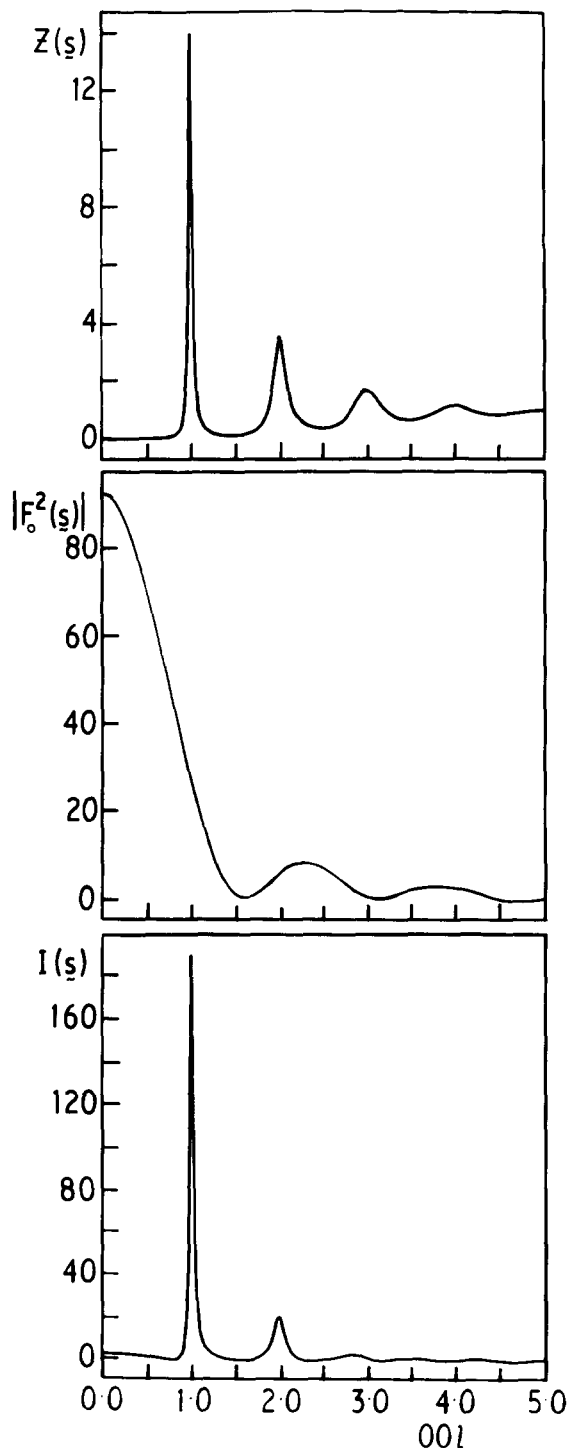


Fig. 9. Diagrams illustrating disordered reciprocal lattices  $Z(s)$  and the corresponding diffraction patterns,  $I(s)$ , produced when multiplied by  $|F_0^2(s)|$ . The calculations are for  $c = 9.6 \text{ \AA}$  and  $d = 15.0 \text{ \AA}$ . The value of  $\delta$  is 1.25 corresponding to a half width in the lattice disorder of about  $\pm 10\%$

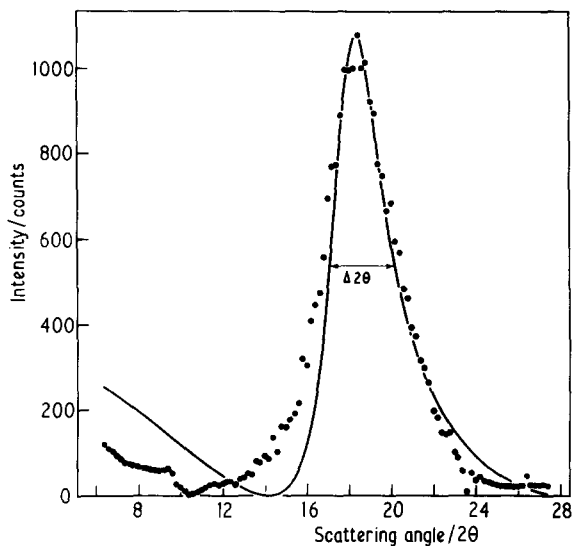


Fig. 10. Analysis of an (001) diffraction reflection of lithium montmorillonite at RH = 76%,  $d = 15.1 \text{ \AA}$ ,  $\bullet$  = observed data. Full width at half maximum (FWHM) =  $\Delta(2\theta) = 3.2^\circ$ . — = line calculated using the disordered lattice model. The disorder parameter,  $\delta$ , is the same as for Figure 9.

fracted intensity. The diffraction pattern is constructed by calculating the Fourier transform of the disordered lattice to reciprocal space and multiplying this by the square of the structure factor for a single platelet. The details of the calculation are given in the Appendix, Part 3. Examples of the reciprocal lattice,  $Z(s)$ , the structure factor  $|F_0^2(s)|$ , and the final pattern,  $I(s)$  are shown in Figure 9 for a particular value of the disorder parameter  $\delta$ .  $|s| = (2/\lambda)\sin \theta$ .

As well as explaining why higher orders of reflection are weak, the model adequately explains the width and asymmetry of the first order reflection. A comparison of calculated and observed diffraction patterns is shown in Figure 10. The best fits to the shape of the (001) reflection are obtained with values of  $\delta$  which suggest that the basal spacing frequently varies by  $\pm 10\%$ . Within the model this could be caused either by wedge-like channels or by variation in the spacing between parallel platelets. The basal spacings for one, two, and three layers of water are 12, 15, and 18  $\text{\AA}$  respectively.

For the two-layer case, a Gaussian distribution of 10% gives a spread of lattice parameters from about 13.5 to 16.5  $\text{\AA}$ . This is not large enough for there to be significant contributions from regions with one and three layers of water. The fit of this distribution to the observed diffraction patterns shows that the number of water layers is reasonably well defined, at least on the plateaus of Figure 6. If the spread of lattice spacing were much greater, say 20%, there would be strong overlap of the distributions corresponding to one, two, and three water layers over the whole range of relative humidity. Such a breakdown is likely in the regions of

the steps of Figure 6, for example, for a Li sample at 47% relative humidity.

Because of the large ratio of diameter to thickness of the platelets it is likely that there will be regions where the platelets fold or buckle as in (C), Figure 1. Such regions of gross folding will also reduce the definition of the diffraction pattern. Güven (1975) has calculated that as the average radius of bending falls below 500 Å the (00 $l$ ) reflections disappear rapidly. Even for bending radii above 1000 Å there is a significant effect on the diffraction pattern. Since this effect is continuous in  $s$  it will also change the shape of broad diffraction lines. Saxena and Schoenborn (1977) have formulated the effect of vertical beam height and divergence with mosaic spread in the sample on the intensity of observed reflections. Using their equations and the observed mosaic widths obtained in this work for the clay-water samples, it is expected that the intensity of the (001) will be depleted by ~55% and the (002) by ~76% of their calculated values. This effect increases for higher orders of diffraction. This will produce an additional correction factor to our model which will necessarily improve the fit of both calculated intensities and line shapes to the experimental data.

It can be seen from Figure 9 that the model predicts a flat signal at high values of  $s$ . In principle, the observed height of the 'background' could be used as an extra parameter to be fitted by the model. In practice it is not easy to separate this contribution from diffuse scattering, incoherent scattering from protons, and low intensity powder diffraction in between Bragg peaks.

Though it is not possible to separate the effects of folding and stacking faults on the diffraction pattern, the interpretation through the one-dimensional distorted lattice model gives a more precise description of the system than one based on particle size effects. A similar conclusion was reached by Kodama et al. (1971) in their analysis of the X-ray diffraction of microcrystalline muscovites.

The interpretation of the rocking curve is that the mosaic spread of the particles in the system is not flat, as it would be for a random powder, and is not sharply peaked, as it would be for a perfectly ordered polycrystal. The corrected distribution is accounted for by a constant 'background' with a Gaussian above it.

Electron microscopy of dilute montmorillonite sols shows extensive polydispersity of platelet diameters. Similar experiments on compressed samples also show a lot of folds (Figure 2). It is now suggested that the peaked feature in the rocking curve can be attributed to the packing of the larger platelets parallel to the plane of the sample. Folds, wedge-like channels and misorientation of the particle-like regions contribute to the Gaussian distribution. The flat contribution to the rocking curve can only come from randomly oriented stacks of platelets. Parts of the sample most likely to be ran-

domly oriented are (B) and (C) in Figure 1. The former in turn will be associated with the small platelet fraction of the clay and may be the cause of folding faults through edge to face interactions.

The interpretation of the flat contribution to the rocking curve given above, is confirmed by the D11 experiment which gives the complete Debye-Scherrer ring in the transmission diffraction pattern. This can be explained only by the presence of randomly oriented groups of particles each consisting of several platelets.

At low water spacings used for these experiments (one to three layers) there are no differences in platelet packing for montmorillonite containing either Li, Na, K, or Cs as exchanged cation. The only difference is the variation of the basal spacing with relative humidity. For K and Cs the transition from one to two to three layers of water is much less sharp than for Li and Na (Mooney et al., 1952). This does not seem to be associated with any fundamental differences in the structure. Neutron small angle scattering experiments at much higher water content (in the sol) indicate that with increasing amounts of water the nature of the cation does affect the relative arrangement of the clay platelets.

The method of preparation might be expected to affect the distribution of the larger platelets, the order parameter  $\delta$  (spread in basal spacings), the fraction of randomly oriented material and the quality of its packing. No difference has been found in the first two properties in samples prepared by compression and suction. It seems probable from the D11 results that the quality of packing in the powder fraction is much improved by compression. Compression redistributes platelets from grossly distorted regions increasing the fraction of randomly oriented stacks of material. In both kinds of sample the randomly oriented fraction is small, about 8%.

#### ACKNOWLEDGMENTS

We thank Dr. G. Zaccai (I.L.L. Grenoble) for his help and advice. This research was supported by the Science Research Council of Great Britain.

#### APPENDIX

##### Part 1

The law governing the attenuation of the neutron beam is assumed to have the form:

$$I_{/l_0} = \exp(-\mu l) \quad (1)$$

$\mu$  is the linear absorption coefficient,  $l$  is the path length through the sample.  $I_{/l_0}$  is the relative intensity of the unscattered beam.

A pencil beam of neutrons, formed by screening the normal beam with cadmium slits, is produced. For the same monitor count in each position, the sample is held at angles to the fine beam so as to present path lengths

directly through the sample which are integer values of  $\bar{l}$ . Here  $\bar{l}$  is the average thickness of the sample and so  $l = n\bar{l}$ . (With the plane of the sample at  $90^\circ$  to the incident beam,  $n = 1$ , and for the sample at  $30^\circ$ ,  $n = 2$  and so on.) A plot of  $\ln(I_{i/l_0})$  against  $n$  has a gradient of  $-\mu\bar{l}$ . The quantity  $\mu\bar{l}$  is used for the attenuation correction. It is not necessary and in any case not of use to separate  $\mu$  and  $\bar{l}$  because  $\bar{l}$  cannot be measured accurately.

Part 2

Correction for attenuation of the beam passing through the sample is taken from the general approach of Buerger (1967). Consider the sample to be divided up into  $n$  subunits, labelled  $i$ . The transmission factor,  $T$  is:

$$T = 1/n \sum_{i=1}^n \exp[-\mu(t_{i1} + t_{i2})] \tag{2}$$

where  $t_{i1}$  is the path length of the incident beam in the sample before scatter and  $t_{i2}$  is the path length of the scattered beam in the sample. For an arbitrarily shaped sample  $(t_{i1} + t_{i2})$  will be a function of the sample's orientation to both incident and scattered beams. For disk samples with radius  $R$  very much greater than their thickness  $\bar{l}$ , equation (2) can be simplified. Dividing the radius into  $n_R$  units and the thickness by  $n_l$  units, since  $R \gg \bar{l}$  then  $n_R \gg n_l$ . We can then write (2) as

$$T = \exp[-\mu(t_1 + t_2)] \tag{3}$$

For plane samples rotating at an angle  $\omega$  and sampling the scattered beam at an angle  $2\theta$ , both with respect to the incident beam, we can separate three scattering configurations shown in Figure 11. Expressions giving the angular dependence for the three cases are:

$$1. \quad t_1 = \frac{\bar{l}}{2} \cdot 1/\sin|\omega|$$

$$t_2 = \frac{\bar{l}}{2} \cdot 1/\sin(2\theta + |\omega|) \tag{4}$$

$$2. \quad t_1 = \frac{\bar{l}}{2} \cdot 1/\sin|\omega|$$

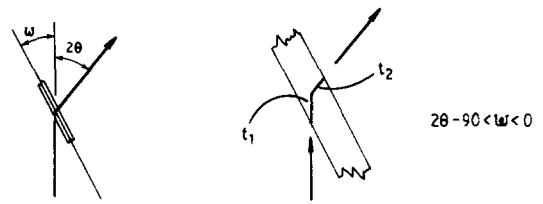
$$t_2 = \frac{\bar{l}}{2} \cdot 1/\sin(2\theta - |\omega|) \tag{5}$$

$$3. \quad t_1 = \frac{\bar{l}}{2} \cdot 1/\sin|\omega|$$

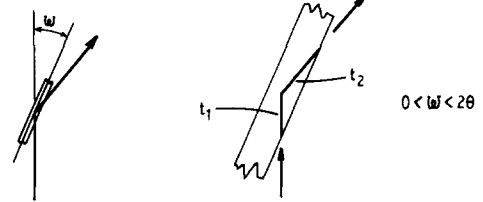
$$t_2 = \frac{\bar{l}}{2} \cdot 1/\sin(|\omega| - 2\theta) \tag{6}$$

To correct the intensity measured at any  $(\omega, 2\theta)$ ,  $I_m(\omega, 2\theta)$ , divide  $I_m(\omega, 2\theta)$  by  $T(\omega, 2\theta)$ . The correction becomes unreliable very close to  $\omega \approx 0$  and  $\omega \approx 2\theta$  and corrections have not been made in these regions of  $\omega$ . In equations (3)–(6) only the product  $\mu\bar{l}$  appears and it

Configuration 1



Configuration 2



Configuration 3

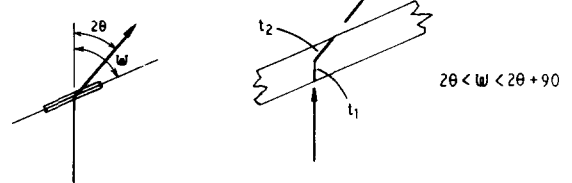


Fig. 11. Diagram to illustrate three configurations where attenuation in plane samples is significant. The detector is at an angle of  $2\theta$  to the incident beam and is fixed. The plane of the sample rotates through  $\omega$ . The variation of  $t_1$  and  $t_2$  with  $\omega$  and  $2\theta$  is shown.

is this quantity that is measured by the method in Part 1 of the Appendix.

Part 3

The calculation of the one dimensional distorted lattice is taken from Guinier (1963). A diffraction pattern of  $(00l)$  reflections may be represented mathematically as

$$I(s) \propto |F_0^2(s)| \cdot Z(s) \cdot A(s) \tag{7}$$

where

$$|s| = (2/\lambda) \sin \theta,$$

$I$  is the intensity,  $F_0$  represents the structure factor of the unit cell,  $Z$  is the reciprocal lattice and  $A$  takes into account instrumental factors such as attenuation and Lorentz factors. This is to be compared with the formulation of  $I_{hk}(s)$  presented by Plançon and Tchoubar (1977). By suitable choice of  $F_0$  and  $Z$  we can construct a diffraction pattern  $I$ . The simplest form for  $F_0$  for the clay plate is a two-sided, Heaviside function:

$$F_0(x) = \begin{cases} 0 & |x| > c/2 \\ 1 & |x| < c/2 \end{cases} \tag{8}$$

$x$  is the real dimension and  $c$  is the thickness of the clay plate. This form of  $F_0$  is chosen for two reasons. First it adequately represents the neutron scattering profile across the clay-water system's unit cell and second the transform of  $F_0(x)$  to reciprocal space,  $F_0(s)$  is well known:

$$\int_{-\infty}^{\infty} F_0(x) \cdot \exp(-2\pi isx) dx = c \cdot \sin(\pi sc) / (\pi sc) \quad (9)$$

The model for  $Z$  is taken directly from Guinier (1963).  $\delta$  is a parameter which characterizes  $h(x)$ , which is the distribution function of the distances between neighboring points on the lattice.  $Z(s)$  has an analytical form provided  $h(x)$  is chosen to be a Gaussian with a full width at half maximum of  $\delta/0.85$ .  $\delta$  is defined as:

$$\delta^2 = \int h(x)(x - d)^2 dx \quad (10)$$

## REFERENCES

- Adams, J. M., Reid, P. I., Thomas, J. M. and Walters, M. J. (1976) On the hydrogen atom positions in a kaolinite; formamide intercalate: *Clays & Clay Minerals* **24**, 267-269.
- Anderson, D. M. (1966) The interface between ice and silicate surfaces: *J. Colloid Interface Sci.* **25** (2), 174-191.
- Aylemore, L. A. G. (1977) Microporosity in montmorillonite from nitrogen and carbon dioxide sorption: *Clays & Clay Minerals* **25**, 148-154.
- Barclay, L. and Ottewill, R. H. (1970) Measurement of forces between colloidal particles: *Spec. Discuss. Faraday Soc.* **1**, 138-147.
- Brown, G. (Editor) (1961) *The X-ray Identification of Crystal Structures of Clay Minerals*: Mineral. Soc., London.
- Buerger, J. (1967) *Crystal Structure Analysis*, p. 217: Wiley, New York.
- Callaghan, I. C. and Ottewill, R. H. (1974) Interparticle forces in montmorillonite gels: *Discuss. Faraday Soc.* **57**, 110-118.
- Cebula, D. J., Thomas, R. K., Harris, N. M., Tabony, J. and White, J. W. (1978) Neutron scattering from colloids: *Discuss. Faraday Soc.* **65** (in press).
- Diamond, S. (1971) Microstructure and pore structure of impact-compacted clays: *Clays & Clay Minerals* **19**, 239-249.
- Fink, D. H. (1977) Internal surface area of Wyoming Bentonite from swelling relationships: *Clays & Clay Minerals* **25**, 196-200.
- Graham, J. (1964) Adsorbed water on clays: *Rev. Pure Appl. Chem.* **14**, 81-90.
- Guinier, A. (1963) *X-ray Diffraction*, pp. 143, 265: Freeman and Co. San Francisco.
- Güven, N. (1975) Evaluation of bending effects of diffraction intensities: *Clays & Clay Minerals* **23**, 272-277.
- Haywood, B. C. G. and Worcester, D. L. (1973) A simple neutron guide tube and diffractometer for small-angle scattering of cold neutrons: *J. Phys. E.* **6**, 658-671.
- Hougardy, J., Stone, W. E. and Fripiat, J. J. (1976) NMR study of adsorbed water. I. Molecular orientation and protonic motions in the two layer hydrate of a Na vermiculite: *J. Chem. Phys.* **64** (9), 3840-3851.
- Institut Laue-Langevin (1977) Neutron beam facilities at the HFR available for users: Institut Laue-Langevin, Grenoble, France.
- Jacrot, B. (1976) The study of biological structures by neutron scattering from solution: *Rep. Prog. Phys.* **39**, 911-953.
- Keren, R. and Shainberg, I. (1975) Water vapor isotherms and heat of immersion of Na/Ca-montmorillonite systems—I: homoionic clay: *Clays & Clay Minerals* **23**, 193-200.
- Kodama, H., Gatineau, L. and Meyring, J. (1971) An analysis of X-ray diffraction line profiles of microcrystalline muscovites: *Clays & Clay Minerals* **19**, 405-413.
- Mitchell, W. A. (1953) Oriented-aggregate specimens of clay for X-ray analysis made by pressure: *Clay Miner. Bull.* **2**, 76-77.
- Mooney, R. W., Keenan, A. G. and Wood, L. A. (1952) Adsorption of water vapor by montmorillonite. I. Heat of desorption and application of BET theory: *J. Am. Chem. Soc.* **74** (6), 1367-1371. II. Effect of exchangeable ion and lattice swelling as measured by X-ray diffraction: *J. Am. Chem. Soc.* **74** (6), 1371-1375.
- Norrish, K. (1954) The swelling of montmorillonite: *Discuss. Faraday Soc.* **18**, 120-134.
- O'Brien, F. E. M. (1948) The control of humidity by saturated salt solutions: *J. Sci. Instrum.* **25**, 73-76.
- Plançon, A. and Tchoubar, C. (1977) Determination of structural defects in phyllosilicates by X-ray powder diffraction. I. Principle of calculations of the diffraction pattern: *Clays & Clay Minerals* **25**, 430-435. II. Nature and proportion of defects in natural kaolinites: *Clays & Clay Minerals* **25**, 436-450.
- van Olphen, H. (1977) *An Introduction to Clay Colloid Chemistry*, 2nd edition: Wiley, New York.
- Rowell, D. L. (1965) Influence of positive charge on the inter- and intra-crystalline swelling of oriented aggregates of Na montmorillonite in NaCl solutions: *Soil Sci.* **100**, 340-347.
- Saxena, A. M. and Schoenborn, B. P. (1977) Correction factors for neutron diffraction from lamellar structures: *Acta Crystallogr.* **A33**, 813-818.
- Schmatz, W., Springer, J., Schelten, J. and Ibel, K. (1974) Neutron small-angle scattering: Experimental techniques and applications: *J. Appl. Crystallogr.* **7**, 96-116.
- Shaw, H. F. (1972) The preparation of oriented clay mineral specimens for X-ray diffraction analysis by a suction-onto-tile method: *Clay Miner.* **9**, 349-350.
- Taylor, R. and Norrish, K. (1966) The measurement of orientation distribution and its application to quantitative X-ray diffraction analysis: *Clay Miner.* **6**, 127-142.
- Tchalenko, J. S., Burnett, A. D. and Hung, J. J. (1971) The correspondence between optical and X-ray measurements of particle orientation in clays: *Clay Miner.* **9**, 47-70.
- Williams, D. G. and Garey, C. L. (1974) Crystal imperfections with regard to direction in kaolinite mineral: *Clays & Clay Minerals* **22**, 117-125.
- Willis, B. T. M. (Editor) (1972) *Chemical Applications of Thermal Neutron Scattering*: Oxford University Press, Oxford.



Резюме- Описывается использование нейтронной дифракции для определения некоторых структурных свойств систем монтмориллонит-вода при низкой концентрации воды. Образцы приготавливались с помощью сжатия или высасывания, чтобы получить образцы глины, содержащие от одного до трех молекулярных слоев воды между пластинками.

Около 10% пластинок в глинах ориентированы беспорядочно. Остальные частично ориентированы в плоскости образца, с углом рассеивания в  $40^\circ$  к средней ориентации. Было предположено, что эти ориентированные домены формируются из больших пластин, присутствующих в системе. Диаграмма дифракции Брэгга лучше объясняется моделью беспорядочной решетки, чем смешанной моделью с небольшими частицами, имеющими определенный параметр решетки. Мы привели в количественное соответствие как интенсивности отражений (001), так и форму отражений (001) с моделью, которая дает примерно среднее значение для рассеивания Гауссиана, характеризующего промежутки между пластинками. Половина ширины рассеивания составляет около 10% параметра решетки.

Не было обнаружено значительных структурных различий между Li, Na, K и Cs монтмориллонитами. Метод приготовления не влияет на структурные свойства больших пластинчатых частиц, но воздействует на беспорядочно ориентированную фракцию. Параметр решетки последней, по видимому, лучше определен для образцов, приготовленных с помощью сжатия.

Опыты по изменению параметра решетки в зависимости от влажности указывают, что структурная модель, которую мы использовали, отвечает требованиям, за исключением таких влажностей, когда в системе наблюдаются изменения слоев воды от 1 до 2 или от 2 до 3.

Kurzreferat- Die Benutzung von Neutronendiffraktion für die Bestimmung von einigen strukturellen Eigenschaften von Montmorillonit-Wasser Systemen bei niedrigen Wasserkonzentrationen wird beschrieben. Die Proben wurden durch Kompression oder Saugen präpariert, um Tonproben mit einer bis drei Molekülschichten von Wasser zwischen den Platten zu ergeben. Ungefähr 10% der Plättchen in dem Ton sind nicht geordnet. Der Rest ist teilweise in der Ebene der Probe angeordnet mit einer Winkelspanne von  $40^\circ$  um die mittlere Orientierung. Es wird vorgeschlagen, daß diese geordneten Bereiche von den im System anwesenden, größeren Plättchen geformt werden. Das Muster der Braggschen Diffraktion kann besser mit einem nicht geordneten Gittermodell erklärt werden als mit einem gemischten Modell, welches kleine Teilchen mit gut definierten Gitterabständen besitzt. Wir haben sowohl die Intensitäten der (001) Reflexionen wie auch die Ausmaße der (001) Reflexion quantitativ einem Modell angepaßt, welches eine Gaußsche Verteilung der Plättchenabstände zulässt. Die Halbwerte der Verteilung ist etwa 10% der Gitterabstände. Keine bedeutenden strukturellen Unterschiede wurden unter Li, Na, K und Cs Montmorilloniten gefunden. Die Art der Ausführung der Präparation hat keinen Effekt auf die strukturellen Eigenschaften der großen Plättchen, beeinflusst jedoch den nicht geordneten Anteil. Der Gitterabstand der letzteren scheint besser definiert zu sein für Proben, die durch Kompression hergestellt werden. Experimente mit der Variation der Gitterabstände mit Luftfeuchtigkeit deuten an, daß das strukturelle Modell, mit Ausnahme von Luftfeuchtigkeiten, bei denen das System von 1 auf 2 oder 2 auf 3 Wasserschichten überwechselt, hinreichend ist.

Résumé-L'emploi de la diffraction de neutrons pour déterminer certaines propriétés de la structure des systèmes montmorillonite-eau à de basses concentrations d'eau est décrite. Les échantillons ont été préparés soit par compression, soit par aspiration, pour donner des échantillons d'argile ayant entre un et trois feuillets moléculaires d'eau entre les plaquettes. A peu près 10% des plaquettes dans l'argile sont orientées au hasard. Le reste est partiellement orienté dans le plan de l'échantillon, avec une envergure d'angle de  $40^\circ$  par rapport à l'orientation moyenne. Il est suggéré que ces domaines sont formés par les plus grandes plaquettes présentes dans le système. Les diagrammes de diffraction de Bragg sont mieux expliqués par un modèle de réseau cristallin désordonné que par un modèle de mélange contenant de petites particules ayant une périodicité d'édifice cristallin bien déterminée. Nous avons quantitativement ajusté à la fois les intensités des réflexions (001) et la forme des réflexions (001) à un modèle qui permet une envergure de Gauss à la périodicité de plaquettes autour d'une valeur moyenne. La moitié de la largeur de cette envergure est d'environ 10% de la périodicité du réseau cristallin. Il n'a été trouvé aucune différence significative de structure entre les montmorillonites Li, Na, K et Cs. La méthode de préparation n'a aucun effet sur les propriétés de la structure des particules à larges plaquettes, mais affecte la partie orientée au hasard. La périodicité du réseau cristallin de cette partie semble mieux définie dans les échantillons préparés par compression. Des expériences sur la variation de la périodicité de l'édifice cristallin due à l'humidité indiquent que le modèle que nous avons employé est adéquat sauf à des humidités où le système change d'une à deux, ou de deux à trois couches d'eau.